Characterizing the dynamic movement of thunderstorms using VLF/LF total lightning data over the Pearl River Delta region

Si Cheng[1], Jianguo Wang[1], Li Cai[1], Mi Zhou[1], Yijun Huang[1], Rui Su[1], Quanxin Li[1]

[1] Electricity Engineering and automation, Wuhan University, Wuhan, 430072, China

Correspondence to: Jianguo Wang (wjg@whu.edu.cn)

Abstract. This paper reveals the characteristics of thunderstorm dynamic movement using total lightning data obtained from the VLF/LF measurement. Eight thunderstorms, which was evenly distributed in the morning, midday, afternoon and evening, are selected to compare the different kinematic features around the Pearl River Delta (PRD) region in the south of China from 17 May to 23 May 2014. The connected-neighborhood labeling method is used to identify lightning clusters and obtain the centroids. Significant characterization parameters are put forward as metrics to reveal the kinematic features of thunderstorms, including the duration, valid area (VA), velocity, direction, and farthest distance in longitude and latitude during the life cycle of storm. A common trend is that the storms initiate in the west of the PRD region, moving to the east and disappearing after the thunderstorm travels around 106.5 km in longitude. There are two kinds of distribution to depict the property of valid area, which are one-peak distribution with the maximum in the mature stage and two-peak distribution with a relatively smaller peak in the early time of storm. The velocity does not show the same trend as the variation of VA which shows the steady increase or decrease during the lifetime of thunderstorm. The biggest VA and highest velocity are 891 km^2 occurred on the evening of 17 May and 204.8 km h^{-1} occurred on the morning of 20 May. The 19 May evening storm was the weakest, with the maximum of VA and velocity being 253 km^2 and 115.3 km h^{-1}, respectively. The motion of storms shows a distinct pattern, as the spread of direction distributes tightly in the range of 0°- 90° and 270°-360°. The movement characteristics of thunderstorm and the associated parameters may help to improve the nowcasting and forecasting system of thunderstorms in this region.

1 Introduction

As one of the noticeable weather events in nature, thunderstorm and its dynamic movement are of great interest in engineering application and in the analysis of interactions between lightning and Earth's atmosphere (Zeng et al., 2016; Jayawardena and Mäkelä, 2021; Kandalgaonkar, 2005). Lightning has been the subject of intense scientific research because of its close relationship with severe weather and convective rainfall, thus posing great threat to the lightning-sensitive

facilities, such as airports, energy sector infrastructure, maritime assets and military bases (Fankhauser, 1971; Villarini and

30   Smith, 2013; Cummins. et al., 1998; Keenan et al., 2000; Lee and Passner, 1993), and the environment (Krider et al., 1980; Lee, 2017). Thunderstorm identification, tracking and short-range forecasting for the future clusters through the lifetime would constitute the basis of severe weather warning operations.

To detect, evaluate, track and forecast thunderstorms, we need a high resolution observation system, and automatic algorithms applied to these data, to obtain quantitative information on the position, size, path and velocity of the cell (Bonelli

35   and Marcacci, 2008). The evaluation of thunderstorm occurrence and characteristics is conducted through the lightning data (Kohn et al., 2011; Meyer et al., 2013), the radar data (Miller and Mote, 2017; Del Moral et al., 2018), or the combination of both (Rigo et al., 2010; Bonelli and Marcacci, 2008; Meyer et al., 2013b; Lu et al., 2021). The lightning detection methods include the ground-based systems, such as the LINET (Betz et al., 2008), Earth Networks Total Lightning Network (ENTLN, Ringhausen and Bitzer, 2021), ZEUS (Kohn et al., 2011) and Lightning Mapping Array (LMA, Weiss et al., 2012), and the

40   space-based satellites, such as the Lightning Image Sensor (LIS, Chronis and Koshak, 2017; Zhang et al., 2019), Optical Transient Detector (OTD, Buechler et al., 2000; Christian, 2003) and Geostationary Lightning Mapper (GLM, Goodman et al., 2013; Rutledge et al., 2020). The reflectivity images provided by the Weather Surveillance Radar (WSR) are commonly used to identify those areas of convection in certain time interval. Due to its ability to capture the spatial and temporal variability of thunderstorm, high resolution radars allow for a detailed analysis of the forming and movement of convection

45   storms (Muñoz et al., 2018). After the recognition of high reflectivity areas or high lightning density areas with automatic algorithms, the motion of thunderstorms can be tracked and extrapolated.

Statistics and comparisons of storm attributes, such as the direction and speed of movement or cell sizes and severity, are studied by many researchers. A cell-based analysis shows that different synoptic conditions are typically associated with specific cell characteristics (Wapler and James, 2015). There is a significant dependence between various cell attributes and

50   the synoptic patterns. E.g., those types associated with broadly westerly flow tend to have high cell speeds and a relatively narrow distribution of cell directions. Those storms which have lower average cell speeds tend to have a higher likelihood of hail. The comparison of storm speed done as a function of the month of the year is conducted between the winter and summer storms (Kohn et al., 2011), showing that the summer ones are much faster than the winter ones, which might be in contradiction with the assumption of faster storms in the winter due to the strengthening of the jet stream at this time . The

55   possible reason is that the summer storms are convective in nature and therefore more intense and faster. Lightning parameter's relationship to Hurricane Harvey's intensification is conducted based on a merged lightning data set consisting of lightning detected by the ground-based ENTLN and space-borne GLM (Ringhausen and Bitzer, 2021). In the rainband and eyewall region, nearly all GLM flash characteristics show a large increase just prior to rapid intensification, with the flash duration, number of events, and groups comprising a flash showing the largest increases. However, up to now, there have

60   been few formal studies that individually analyse such fundamental components in each single thunderstorm. It is the objective of this study to address the aforementioned.

The purpose of this paper is to provide a comprehensive kinematic feature of thunderstorms over the PRD region in the perspective of the distribution of total lightning data obtained from VLF/LF Foshan Total Lightning Location System. We conduct a detail analysis about the temporal and spatial evolution by eight cases occurred within a week during 17 May to 23 May 2014. The 8-adjacent connected-neighborhood labeling algorithm is applied for the identification of clusters during the life time of thunderstorm, through which the centroids and valid areas are figured out in every 12-minute time interval. To characterize the spatial evolution, five parameters are put forward to quantify the movement of clusters in various periods of a day. The result shows that there is a clear pattern in terms of the transition of thunderstorms in this region.

2 Instrument and methodology

2.1 Foshan total lightning location system

In the summer of 2013, 3-demention Foshan total lightning location system (FTLLS) was installed in Guangdong Province, China (Cai et al., 2019; Cai, 2013). Based on the electromagnetic environment, surrounding buildings, terrain conditions, communication conditions, etc., nine sub-station was deployed to detect lightning events over the PRD region, shown in Figure 1. The distance between each sub-station is generally 10 to 40 km and the detection range is more than 100 km. The coverage of the entire station network is about 1000 km^2, which can effectively cover lightning activity in Guangzhou. The DTZ, MCZ and JAZ sub-stations are far apart, forming a longer baseline, which can effectively improve the locating accuracy, while the remaining sub-stations are densely distributed.

All the nine substations are installed on the roof of the building of subsidiaries of Foshan Electric Power Company, China Southern Power Grid. Power supply is achieved via the 220 VAC power network. Wide-band electric field measuring systems with a 3 dB bandwidth from 200 Hz to 500 kHz are employed to measure the lightning electromagnetic impulses. Three-dimension location algorithm is utilized in FTLLS. The location information contains the height of lightning, which can be applied to identify the discharge types. The characteristic parameters of the radiated electric field waveform produced by different type of discharge events can also be served as a discrimination method. The classification of cloud-to-ground flash (CG), intra-cloud flash (IC) and narrow bipolar events (NBEs) can be accomplished by a combined analysis of those parameters from FTLLS. The system can provide real-time lightning data to the electric utility industry, which mainly includes the time of lightning strokes, three-dimension location, peak current, rise time, fall time, pulse width and signal-to-noise ratio. Based on the Monte Carlo simulation, the two-dimensional horizontal location error is basically less than 100 m, and the vertical error (altitude) is less than 200 m when the lightning event occurs within the network. The validation of system has been guaranteed through comparison of rocket-triggered lightning experiment and the application of transmission lines (Wang et al., 2019; Cai et al., 2020).

Atmospheric
Chemistry
and Physics
Discussions

2.2 Methodology

All geographical plots in this paper are created by counting lightning events within 0.01°×0.01°grid boxes, corresponding to an approximate resolution of 1 km over the Pearl River Delta region (112°-115°E, 22°-25°N). If a larger box is employed to count lightning events, more flashes will be contained within each box, leading to ambiguous cluster recognitions.

95 Conversely, smaller resolution results in a great deal of empty boxes, mistakenly separating the thunderstorm clusters. The analysis of total lightning is in progress with the time scale of 12 min which was twice of the adjacent Doppler Radar scans. Connected-neighborhood labeling is applied to grid boxes to identify lightning clusters. Connectivity means that a connected path can be formed between two boxes in the area. From the perspective of digital images, connectivity can be classified as two types: (1) 4-adjacenct connected-neighborhood labeling, which refers to starting at any pixel position in a collection or

100 area and searching from four directions (left, above, right, below) of the pixel, any other pixels can be found in the collection or area; and (2) 8-adjacenct connected-neighborhood labeling, which is the same as 4-adjacent, but adds four diagonal position (Miller and Mote, 2017; Zan et al., 2019; Xue et al., 2019). Connected neighborhood labeling is to give each connected area a unique number during the search process. In this paper, the second type is adopted to automatically identify lightning clusters.

105 The process of thunderstorm visualization is shown in Figure 2. The analysis area is divided into 0.01°×0.01° grid boxes, corresponding to the geographic area of 1 km^2 approximately. The number of individual lightning events is counted within each grid box at 12-minute intervals, on which we rely to draw the lightning density map. Setting one lightning event as the density threshold, the box with more than an event can be defined as a valid box. Using the 8-adjacent connection neighborhood labeling algorithm, we can figure out the number of valid boxes in each thunderstorm cluster. As the area of

110 each box is 1 km^2, we define the number of valid boxes as the valid area (VA). To better capture the main spatial movement of thunderstorm, the clusters less than 25 km^2 and the duration of storm less than 60 min are removed based on the scale of thunderstorms in the PRD region. The final area of each cluster is substituted by equivalent circle (EC). Equation (1) is the conversion formula of VA and the radium of equivalent circle (REC), which is used to draw the ground motion map in the following section.

115 $\text{REC} = \sqrt{\dfrac{\text{VA}}{\pi}}$ (1)

Taking the proportion of lightning frequencies in each grid to the total number of lightning in all effective grids as the weight, the longitude and latitude coordinates of discharge centroid (C) are obtained by the weighted average of each grid in valid area. The expressions are shown in Eq. (2) and Eq. (3).

$C_{\text{lon}} = \sum_{N=1}^{VA}(\dfrac{\text{the number of flashes in Grid N}}{\text{total flashes in valid area}} * N_{\text{lon}})$ (2)

120 $C_{\text{lat}} = \sum_{N=1}^{VA}(\dfrac{\text{the number of flashes in Grid N}}{\text{total flashes in valid area}} * N_{\text{lat}})$ (3)

Atmospheric
Chemistry
and Physics
Discussions

where Clon is the longitude of discharge centroid in the density diagram, Clat is the latitude of discharge centroid, Nlon is the longitude of one gird in all the effective grids in the density diagram, Nlat is the latitude of one gird in all the effective grids.

After calculating the coordinate of discharge centroid, we can obtain the distance that thunderstorm runs and the direction

125   it moves (seen in Eq. (4)). The velocity of clusters, determined by distance traveled in 12-minute time interval, is recorded as well (seen in Eq. (5)). The farthest distances (FD) that the thunderstorm moves in longitude and latitude during the lifetime help to foresee the movement of storm, the expression of which are shown in Eq. (6) and Eq. (7).

$$Direction = \arctan \frac{C_{lat2} - C_{lat1}}{C_{lon2} - C_{lon1}} \quad (0° < \text{Direction} < 360°) \tag{4}$$

$$Velocity = \frac{\sqrt{(C_{lat2} - C_{lat1})^2 - (C_{lon2} - c_{lon1})^2}}{12} * 60 \tag{5}$$

130    $$FD_{lon} = \max(C_{lon}) - \min(C_{lon}) \tag{6}$$

$$FD_{lat} = \max(C_{lat}) - \min(C_{lat}) \tag{7}$$

where the unit of velocity is km h^{-1}.

To characterize the motion of thunderstorm, we use five parameters mentioned above to depict their movements, which include the valid area, velocity, direction, and farthest distance in longitude and latitude. The meaning of parameters is

135   shown in Table 1.

3 Result

3.1 Total lightning characteristics and temporal evolution of thunderstorm

From the thunderstorm activities detected by FTLLS in the summer of 2014, eight thunderstorms around the Pearl River Delta region are selected which were evenly distributed in the morning, midday, afternoon and evening during 17 May to 23

140   May. Table 2 provides the basic information of these thunderstorms, including the date, the specific time, the duration, the total number of lightning events, flash rate (flashes per hour) and flash-type classification. A common trend of the thunderstorms over the PRG region is that convection occurs most frequently during the afternoon due to solar heating (Chen et al., 2014; Chen et al., 2015). The life cycle durations range from 2 hours to 4.2 hours, with a large difference in the number of total lightning.

145   The thunderstorm with highest number of total lightning occurred on the afternoon of 23 May, consisting of 101,242 lightning events within 3.6 hours. The lowest number of total lightning events occurred on the evening of 19 May, lasting for 2.4 hours with 14,926 lightning events in total. The midday and afternoon thunderstorms keep relatively strong and stable, with total lightning more than twelve thousand per hour, while the morning thunderstorms are much gentle and weak, with around ten thousand lightning events per hour. The two evening thunderstorms are much variable and differentiated, with the

150   first case possessing the highest frequency (29,240) per hour and the second case possessing the lowest frequency (7,263)
      per hour.

      In the LLS data set of all storms, IC events make up 81.7% of total lightning and CG events make up 17.5% of total
      lightning. The NBEs make up the very slightest proportion, with less than 1% of total lightning. The 17 May afternoon storm
      consists of 81,872 lightning events, with IC events accounting for the highest proportion (91.8%) among all storms.
155   Distinctly high proportion of IC events occurred on 23 May afternoon storm and 17 May evening storm, which are
      considerably strong storms in eight cases, indicating that high IC ratio is in connection with severe weather. MacGorman et
      al. (1989) suggested that strong and deep updrafts may enhance the production of IC flashes and delay or even suppress the
      production of CG flashes. As the IC flash rate may grow disproportionately from the CG flash rate as storm become more
      severe, the proportion of IC events may reach high values during strong updrafts (Chèze and Sauvageot, 1997; Pineda et al.,
160   2011). However, the weak 21 May morning storm also possesses a high proportion of IC event (88.7%), while other storms
      with similar scale show much lower IC ratio. Overall, the proportion of IC events is variable in thunderstorms, making
      difficult to use them as a tool for predicting severe weather.

      General total lightning distributions with respect to time of eight cases are presented in Fig. 3. The comparison between
      lightning events detected by the FTLLS (green shaded areas) and the chosen thunderstorms (light blue shaded areas) shows
165   that there are some other storms dispersed within the LLS detection area, and the most prominent storms are selected chosen
      to characterize the movements. Note that the light blue shaded area in each statistical time interval were derived within the
      thunderstorm system, the analysis period was defined from the initiation to the dissipating of thunderstorms, when the main
      body of the thunderstorms are well observed by radar. The blue line and red lines represent the IC events and CG events,
      respectively. We can see that the variation of IC events is highly consistent with the total lightning, while the variation of CG
170   events is quite different. The highest IC rates occur at the early stage of the thunderstorms. However, the highest CG rates
      occur at the middle and late stage, indicating that the occurrence of CG events is later than that of the IC events.

3.2 Spatial footprint of thunderstorms

      The visions to the horizon of thunderstorms are displayed in Figure 4. The storm footprint is defined as the combination
      of the unique area consisting of the VA of each cluster and the path of centroid. During the lifetime of all thunderstorms, the
175   horizontal movement of the thunderstorm does not exceed 150 km in longitude and 100 km in latitude, except that the path
      of 18 May afternoon thunderstorm is longer than the average and depicted in 200 km×150 km domain.

      The coverage and intensity of thunderstorms during the whole process can be visually presented in the evolution map. At
      the initiation stage, the VA is much smaller than that in the development or maturation stage when the thunderstorm moves
      faster in the meanwhile. Note that there is some interspace between two centroids when the storms move fast and the VA is
180   not big enough. The reason is that the circle in the map is the equivalent of valid area and can only reflect the value of
      thunderstorm area within 12 min.

The transition of storms is mainly from west to east with long tracks, usually initiating at Foshan district, crossing the Guangzhou district and disappearing at the Dongguan district. However, the 17 May midday storm is inclined to twist and spin in the same place with extremely short tracks. The VA of 19 May evening storm is relatively small in each time interval

185   compare with other storms, which is in accord with the small number of total lightning analyzed above, however, the velocity is no slower than any other severe storms.

3.2 Duration, Valid area, velocity, farthest distance and direction

Figure 5 displays two lightning parameters to characterize the intensity and movement of thunderstorms: valid area and velocity, which can comprehensively show the track of thunderstorm in a measurable way. Despite of the different period of

190   a day, there are two kinds of distribution of thunderstorm valid area in the whole evolution processes. The first distribution is characterized as one-peak seen in Figure 5(a)(e)(g). The valid area shows an upward trend at the beginning and decreases at last. The rise period is found to be longer than the drop period, which means that the peak of VA lies in in the mature stage of thunderstorm. The second distribution is defined as two-peak distribution in Figure 5 (b)(f)(h). The VA increases in the initiation stage and reaches the first peak in the developing stage. After a small decline, the VA surges in a short time and

195   arrives at the second higher peak in the mature stage. At last, the VA decreases rapidly as the thunderstorm is dissipating. Figure 5(c)(d) is not in full accord with one-peak distribution but very close to it. The difference is that the VA shows a slight increase sign after the highest peak. Meanwhile, the peak time of 17 May midday storm is much earlier than the typical one-peak distribution, of which the peak time basically occur in the mature stage. It is noticed that the VA does not decrease to zero at last because of the existence of time interval and the threshold of cluster area.

200   The velocity exhibits more marked changes with time. It oscillates severely compared with the valid area which shows the steady increase or decrease during the lifetime of thunderstorm. There is no stable variation about the velocity of thunderstorm, indicating that instability of convection within the cloud. When the number of lightning events grows up and the valid area becomes bigger in the developing stage and mature stage, the velocity does not show an obvious increase tendency, which is quite different from common cognition about thunderstorms. This finding is of great significance to

205   facilitate the knowledge about the kinematics of mesoscale convection system.

The violin plots in Figure 6 present the cluster attributes including the VA and velocity in the whole thunderstorm processes. The VA boxes in the afternoon show the rugby-shaped distributions, indicating that the storms are variable during the life cycle and extremely severe in the mature stage (seen in Figure 5 (e)(f)). The storm in the morning, midday and evening is much stable and the VA shows the uniform distribution, exhibiting the rectangle-shaped boxes. There is great

210   difference between the two evening storms, with both the biggest and smallest maximum in this period, which is because the instability of convection in this region. The storm with big VA does not mean a fast speed when it moves. The velocity of each storm is densely distributed around the median, with only one value much bigger than others, showing the rugby-

shaped distributions. Although the VA of 17 May evening storm is much bigger than another evening storm, the speed does not greatly discriminate between each other.

215   Five characterization parameters are listed in Table 3 to reveal the kinematic features of thunderstorms. The maximum VA represents the biggest coverage that the thunderstorm affects within a 12-minute interval. The afternoon storm is notably more severe and intense than that in the morning and midday, while the two evening storms distinguish greatly with each other. The maximum VA is 891 km^2 occurred on the evening of 17 May, with the mean value being 662.7 km^2. However, the storm with minimum VA also occurs on the evening of 19 May, the maximum and mean of which are 253 km^2

220   and 146.7 km^2, respectively. It can be found that the velocity does not match precisely with the VA. The storm with highest speed occurred on the morning of 20 May, with the value of 204.8 km h^{-1}. The lowest maximum of speed was 115.3 km h^{-1} occurred on the evening of 19 May. Although total lightning events of these two storms are the smallest two among eight cases, but the speed of cluster does not show the same characteristic.

To measure the horizontal motion of thunderstorms during the whole process, the horizontal farthest distances (FD) in

225   longitude and latitude are calculated by the coordinates of centroids. It can be clearly seen that the longitudinal FD is much longer than the latitudinal FD, which means that movement of storm is mainly along the east-west path. The maximum and the minimum FD in longitude are 153 km and 55 km, respectively. The FD in latitude are much shorter than that in longitude, with the maximum and minimum being 45 km and 12 km.

Figure 7 illustrates the direction of cluster. We gathered the direction of all cases in the normalized timeline to show the

230   orientation. The motion of storms shows a distinct pattern, as the spread of direction distributes tightly in the range of 0°-90° and 270°-360°. Combining with the ground track of thunderstorms in Figure 6, we can clearly see that the storms initiate in the west of the PRD region, moving to the east and disappearing after the thunderstorms travel around 106.5 km. This kinetic information could shed light on the further research on severe convection weather prediction.

4 Discussion and Conclusion

235   For the purpose of characterizing the dynamic movement of thunderstorms as well as the associated attributes of lightning clusters over the PRD region, we investigate eight cases occurred within a weak from 17 May to 23 May in 2014. Based on the high resolution total lightning data set obtained from VLF/LF Foshan Total Lightning Location System, the temporal and spatial characteristics of thunderstorms are presented in this study. To analyze the thunderstorm cluster features, statistics of various cluster parameters have been calculated.

240   Using 8-adjacenct connected-neighborhood labeling algorithm, five parameters are put forward to measure thunderstorm kinematics features, including the duation, valid area, velocity, direction and farthest distance in longitude and latitude. Table 4 shows the parameters comparison between eight cases in the PRD region and previous studies. Various thresholds are setted to better capture the movement of thunderstorms. Miller and Mote (2017) identified the thunderstorm as the region

of contiguous radar reflectivity greater than or equal to 40 dBz using connected neighborhoods labeling. A sophisticated

245 approach was taken to identify the rainfall pixels by Rigo et al. (2010) who used the radar reflectivity, piexl area and duation

as the thresholds. A lower reflectivity threshold of 12 dBz was chosen to ensure all possible clusters, while the threshold of

other parameter can appropriately aviod non-precipitation echoes in the rainstorm. In this paper, the valid box less than one

flash, the area of clusters less than 25 km^2 and the duration of storm less than 60 min are neglected to reduce the amount of

small ground clusters and track the main storms within the analysis region.

250 Eight thunderstorms, which was evenly distributed in the morning, midday, afternoon and evening, are selected to

compare the different kinematic features from 17 May to 23 May 2014. Most of previous studies focus on the interannual or

interdecadal variations in the characteristics of the storms. Kohn et al. (2011) selected 670 winter storms and 13,600

summer storms in 2008 to track the spatial and temporal attributes over the Mediterranean area and the Europe. Harrison and

Karstens (2017) climatologically analysis the fundamental components of thunderstorm geospatial movements within the

255 continental United States. This paper is aim to make a comprehensive analysis about the cases in a week and reveal the

dynamic motion of thundestrom over the PRD region in the south of China.

Significant characterization parameters are proposed as metrics to depict the kinematic features of thunderstorms,

including the duration, VA, velocity, direction, and FD in longitude and latitude during the evolution of thunderstorm. It is

found that no more than three thunderstorm parameters are demonstrated in the previous study. Rigo et al. (2010) reported

260 the duration and the average area of 66 Catalonia warm season thunderstorms. The lifetime was between 54 min to

approximately 8h, with the mean duration being about 3.5 h, which is a slight longer than this study. The average area was

509 km^2 in 6-minute time interval, with the biggest cluster area in the mature stage. A June supercell propagated north of

Munich in eastern direction was reported by Meyer et al. (2013b) to illustrate the area, velocity and farthest distance of

storms, showing that the maximum of cell area was nearly 500 km^2 in 15-min interval.

265 In this paper, there are two kinds of distribution to describe the variation of valid area during the lifetime of

thunderstorms, which are one-peak distribution with the maximum in the mature stage and two-peak distribution with a

relatively smaller peak in the early time of storm. The maximum VA is 891 km^2 occurred on the evening of 17 May, with the

mean value being 662.7 km^2. The storm with minimum VA also occurs in the evening, the maximum and mean of which are

253 km^2 and 146.7 km^2, respectively. The variation of Meyer's case mentioned above appears to be more likely two-peak

270 distribution, with a sharp decrease in the developing stage. The maximum of cluster areas vary notably between storms

reported by Betz et al. (2008), the largest area reaches up to 7000 km^2 in 10 min, while the smallest area is only 1550 km^2.

The intensity of storms discriminates in different period of a day in this paper, but not in a big difference, indicating that the

convection in the summer season is sereve but stable in this region. To be noted, the valid area observed by the FTLLS is

much smaller than that observed by the radar, where the former represents the lightning discharge acitivity and electricity

275 charge accumulation, and the latter reflects the content of hydrometeors and the effect to radar echoes (Rigo et al., 2010;

Miller and Mote, 2017).

The velocity of thunderstorm obtained by the motion of lightning centroids in this paper represents the integral movement which is basically composed by three types of factors: the translation (synoptic), the forced propagation (mesoscale) and the autopropagation (thunderstorm itself) (Cotton et al., 2011). The storm with highest speed occurred on

280 the morning of 20 May, with the value of 204.8 km/h. The lowest maximum of speed was 115.3 km/h occurred on the evening of 19 May. The velocity does not show the same tendency as the variation of VA during the lifetime of thunderstorms. It oscillates severely compared with the valid area which shows the steady increase or decrease during the lifetime of thunderstorm. This feature is also seen in the Mediterranean storm (Betz et al., 2008), but with a general upward trend in some cells during the whole movement. Meyer et al. (2013b) proposed that long-lived storms are most likely fast

285 propagation as the storms with velocities around 80 km/h spent 150 min to 240 min to cross the domain, however, this was under-represented because of the insufficient statistics. The eight cases in this study also does not show this trend.

Affected by rivers in the Pearl River Delta region, the motion of storms shows a distinct pattern, as the spread of direction distributes tightly in the range of 0°- 90° and 270°-360°, indicating that thunderstorms mainly move from east to west. The direction of thunderstorm in America was quite different from that in the PRD region (Harrison and Karstens,

290 2017). A large uniformed direction of thunderstorm proved to be averaging between 200° and 270° showing the southwest-to-northeast movement. Miller and Mote (2017) found that the topographic relief may be the cause of the thunderstorm orientation.

Overall, the detail analysis of the dynamic movement of thunderstorms shows that there are some remarkable characteristics, but still exist variations among thunderstorms in different periods of a day over the PRD region in the

295 summer season. The result helps to improve the recognition of server thunderstorm in advance by giving a general understanding of how long the storm lasts, how fast the cluster moves and how much area the storm affects, via information about the kinematics features of thunderstorms, and ideally establish a foundation for future research that may contribute to the development of a new or improved prediction paradigm.

300

305

References

310

Betz, H. D., Schmidt, K., Oettinger, W. P., and Montag, B.: Cell-tracking with lightning data from LINET, Advances in geosciences, 17, 55-61, https://doi.org/10.5194/adgeo-17-55-2008, 2008.

Bonelli, P., and Marcacci, P.: Thunderstorm nowcasting by means of lightning and radar data: algorithms and applications in northern Italy, Nat. Hazard. Earth Sys., 8, 1187-1198, https://doi.org/10.5194/nhess-8-1187-2008, 2008.

315 Buechler, D. E., Driscoll, K. T., Goodman, S. J., and Christian, H. J.: Lightning activity within a tornadic thunderstorm observed by the optical transient detector (OTD), Geophys. Res. Lett., 27, 2253-2256, https://doi.org/10.1029/2000GL011579, 2000.

Cai, L.: Ground-based VLF/LF three dimensional total lightning location technology, Ph. D, Wuhan Univerisy, 124 pp., 2013.

320 Cai, L., Zou, X., Wang, J., Li, Q., Zhou, M., Fan, Y., and Yu, W.: Lightning electric‑field waveforms associated with transmission-line faults, IET Generation, Transmission & Distribution, 14, 525-531, https://doi.org/10.1049/iet-gtd.2019.0736, 2020.

Cai, L., Zou, X., Wang, J., Li, Q., Zhou, M., and Fan, Y.: The Foshan Total Lightning Location System in china and its initial operation results, Atmosphere-Basel, 10, 149, https://doi.org/10.3390/atmos10030149, 2019.

325 Chen, X., Zhao, K., Xue, M., Zhou, B., Huang, X., and Xu, W.: Radar-observed diurnal cycle and propagation of convection over the Pearl River Delta during Mei-Yu season, Journal of Geophysical Research: Atmospheres, 120, 12557-12575, https://doi.org/10.1002/2015JD023872, 2015.

Chen, X., Zhao, K., and Xue, M.: Spatial and temporal characteristics of warm season convection over Pearl River Delta region, China, based on 3 years of operational radar data, Journal of Geophysical Research: Atmospheres, 119, 12, 412-447,

330 465, https://doi.org/10.1002/2014JD021965, 2014.

Chèze, J. L., and Sauvageot, H.: Area-average rainfall and lightning activity, Journal of Geophysical Research: Atmospheres, 102, 1707-1715, https://doi.org/10.1029/96JD02972, 1997.

Christian, H. J.: Global frequency and distribution of lightning as observed from space by the Optical Transient Detector, Journal of Geophysical Research, 108, https://doi.org/10.1029/2002JD002347, 2003.

335 Chronis, T., and Koshak, W. J.: Diurnal Variation of TRMM/LIS Lightning Flash Radiances, B. Am. Meteorol. Soc., 98, 1453-1470, https://doi.org/10.1175/BAMS-D-16-0041.1, 2017.

Cotton, W. R., Bryan, G., and van den Heever, S. C.: Chapter 4 - The Parameterization or Modeling of Microphysical Processes in Clouds, in: International Geophysics, edited by: Cotton, W., Bryan, G., and van den Heever, S., Academic Press, 87-142, 2011.

340 Del Moral, A., Rigo, T., and Llasat, M. C.: A radar-based centroid tracking algorithm for severe weather surveillance: identifying split/merge processes in convective systems, Atmos. Res., 213, 110-120, https://doi.org/10.1016/j.atmosres.2018.05.030, 2018.

Fankhauser, J. C.: Thunderstorm-environment interactions determined from aircraft and radar observations, Mon. Weather Rev., 99, 171-192, https://doi.org/10.1175/1520-0493(1971)099<0171:TIDFAA>2.3.CO;2, 1971.

345 Goodman, S. J., Blakeslee, R. J., Koshak, W. J., Mach, D., Bailey, J., Buechler, D., Carey, L., Schultz, C., Bateman, M., McCaul, E., and Stano, G.: The GOES-R Geostationary Lightning Mapper (GLM), Atmos. Res., 125-126, 34-49, https://doi.org/10.1016/j.atmosres.2013.01.006, 2013.

Harrison, D. R., and Karstens, C. D.: A climatology of operational storm-based warnings: A geospatial analysis, Weather Forecast., 32, 47-60, https://doi.org/10.1175/WAF-D-15-0146.1, 2017.

350 Jayawardena, I. M. S. P., and Mäkelä, A.: Spatial and temporal variability of lightning activity in Sri Lanka, Cham, 2021, 573-586, 2021.

K., L. C., E., P. K., and M., D. M.: The US National Lightning Detection Network/sup TM/ and applications of cloud-to-ground lightning data by electric power utilities, IEEE T. Electromagn. C., 40, 465-480, https://doi.org/10.1109/15.736207, 1998.

355 Kandalgaonkar, S. S.: Spatio-temporal variability of lightning activity over the Indian region, Journal of Geophysical Research, 110, https://doi.org/10.1029/2004JD005631, 2005.

Keenan, T., Rutledge, S., Carbone, R., Wilson, J., Takahashi, T., May, P., Tapper, N., Platt, M., Hacker, J., Sekelsky, S., Moncrieff, M., Saito, K., Holland, G., Crook, A., and Gage, K.: The Maritime Continent-Thunderstorm Experiment (Mctex): Overview And Some Results, B. Am. Meteorol. Soc., 81, 2433-2456, https://doi.org/10.1175/1520-
360 0477(2000)081<2433:TMCTEM>2.3.CO;2, 2000.

Kohn, M., Galanti, E., Price, C., Lagouvardos, K., and Kotroni, V.: Nowcasting thunderstorms in the Mediterranean region using lightning data, Atmos. Res., 100, 489-502, https://doi.org/10.1016/j.atmosres.2010.08.010, 2011.

Krider, E. P., Noggle, R. C., Pifer, A. E., and Vance, D. L.: Lightning Direction-Finding Systems for Forest Fire Detection, B. Am. Meteorol. Soc., 61, 980-986, https://doi.org/10.1175/1520-0477(1980)061<0980:LDFSFF>2.0.CO;2, 1980.

365 Lee, J. Y.: System Level Risk Analysis of Electromagnetic Environmental Effects and Lightning Effects in Aircraft: Steady State and Transient, in, edited, 1, ProQuest Dissertations & Theses, Ann Arbor,2017.

Lee, R. R., and Passner, J. E.: The Development and Verification of TIPS: An Expert System to Forecast Thunderstorm Occurrence, Weather Forecast., 8, 271-280, https://doi.org/10.1175/1520-0434(1993)008<0271:TDAVOT>2.0.CO;2, 1993.

Lu, J., Qie, X., Jiang, R., Xiao, X., Liu, D., Li, J., Yuan, S., Chen, Z., Wang, D., Tian, Y., and Yi, X.: Lightning activity
370 during convective cell mergers in a squall line and corresponding dynamical and thermodynamical characteristics, Atmos. Res., 256, 105555, https://doi.org/10.1016/j.atmosres.2021.105555, 2021.

MacGorman, D. R., Burgess, D. W., Mazur, V., Rust, W. D., Taylor, W. L., and Johnson, B. C.: Lightning Rates Relative to Tornadic Storm Evolution on 22 May 1981, Journal of Atmospheric Sciences, 46, 221-251, https://doi.org/10.1175/1520-0469(1989)046<0221:LRRTTS>2.0.CO;2, 1989.

375 Meyer, V. K., Höller, H., and Betz, H. D.: The temporal evolution of three-dimensional lightning parameters and their

suitability for thunderstorm tracking and nowcasting, Atmos. Chem. Phys., 13, 5151-5161, https://doi.org/10.5194/acp-13-5151-2013, 2013a.

Meyer, V. K., Höller, H., and Betz, H. D.: Automated thunderstorm tracking: utilization of three-dimensional lightning and radar data, Atmos. Chem. Phys., 13, 5137-5150, https://doi.org/10.5194/acp-13-5137-2013, 2013b.

380 Miller, P. W., and Mote, T. L.: A Climatology of Weakly Forced and Pulse Thunderstorms in the Southeast United States, J. Appl. Meteorol. Clim., 56, 3017-3033, https://doi.org/10.1175/JAMC-D-17-0005.1, 2017.

Muñoz, C., Wang, L., and Willems, P.: Enhanced object-based tracking algorithm for convective rain storms and cells, Atmos. Res., 201, 144-158, https://doi.org/10.1016/j.atmosres.2017.10.027, 2018.

Pineda, N., Bech, J., Rigo, T., and Montanyà, J.: A Mediterranean nocturnal heavy rainfall and tornadic event. Part II: Total

385 lightning analysis, Atmos. Res., 100, 638-648, https://doi.org/10.1016/j.atmosres.2010.10.027, 2011.

Rigo, T., Pineda, N., and Bech, J.: Analysis of warm season thunderstorms using an object-oriented tracking method based on radar and total lightning data, Nat. Hazard. Earth Sys., 10, 1881-1893, https://doi.org/10.5194/nhess-10-1881-2010, 2010.

Ringhausen, J. S., and Bitzer, P. M.: An In‐Depth Analysis of Lightning Trends in Hurricane Harvey Using Satellite and Ground‐Based Measurements, Journal of Geophysical Research: Atmospheres, 126, https://doi.org/10.1029/2020JD032859,

390 2021.

Rutledge, S. A., Hilburn, K. A., Clayton, A., Fuchs, B., and Miller, S. D.: Evaluating Geostationary Lightning Mapper Flash Rates Within Intense Convective Storms, Journal of Geophysical Research: Atmospheres, 125, https://doi.org/10.1029/2020JD032827, 2020.

Villarini, G., and Smith, J. A.: Spatial and temporal variability of cloud-to-ground lightning over the continental U.S. during

395 the period 1995‐2010, Atmos. Res., 124, 137-148, https://doi.org/10.1016/j.atmosres.2012.12.017, 2013.

Wang, J., Li, Q., Cai, L., Zhou, M., Fan, Y., Xiao, J., and Sunjerga, A.: Multiple-Station Measurements of a Return-Stroke Electric Field From Rocket-Triggered Lightning at Distances of 68‐126 km, IEEE T. Electromagn. C., 61, 440-448, https://doi.org/10.1109/TEMC.2018.2821193, 2019.

Wapler, K., and James, P.: Thunderstorm occurrence and characteristics in Central Europe under different synoptic

400 conditions, Atmos. Res., 158-159, 231-244, https://doi.org/10.1016/j.atmosres.2014.07.011, 2015.

Weiss, S. A., MacGorman, D. R., and Calhoun, K. M.: Lightning in the Anvils of Supercell Thunderstorms, Mon. Weather Rev., 140, 2064-2079, https://doi.org/10.1175/MWR-D-11-00312.1, 2012.

Xue, C., Liu, J., Yang, G., and Wu, C.: A Process-Oriented Method for Tracking Rainstorms with a Time-Series of Raster Datasets, Applied Sciences, 9, 2468, https://doi.org/10.3390/app9122468, 2019.

405 Zan, B., Yu, Y., Li, J., Zhao, G., Zhang, T., and Ge, J.: Solving the storm split-merge problem—A combined storm identification, tracking algorithm, Atmos. Res., 218, 335-346, https://doi.org/10.1016/j.atmosres.2018.12.007, 2019.

Zeng, R., Zhuang, C., Zhou, X., Chen, S., Wang, Z., Yu, Z., and He, J.: Survey of recent progress on lightning and lightning protection research, High Voltage, 1, 2-10, https://doi.org/10.1049/hve.2016.0004, 2016.

Zhang, D., Cummins, K. L., Bitzer, P., and Koshak, W. J.: Evaluation of the Performance Characteristics of the Lightning
410 Imaging Sensor, J. Atmos. Ocean. Tech., 36, 1015-1031, https://doi.org/10.1175/JTECH-D-18-0173.1, 2019.
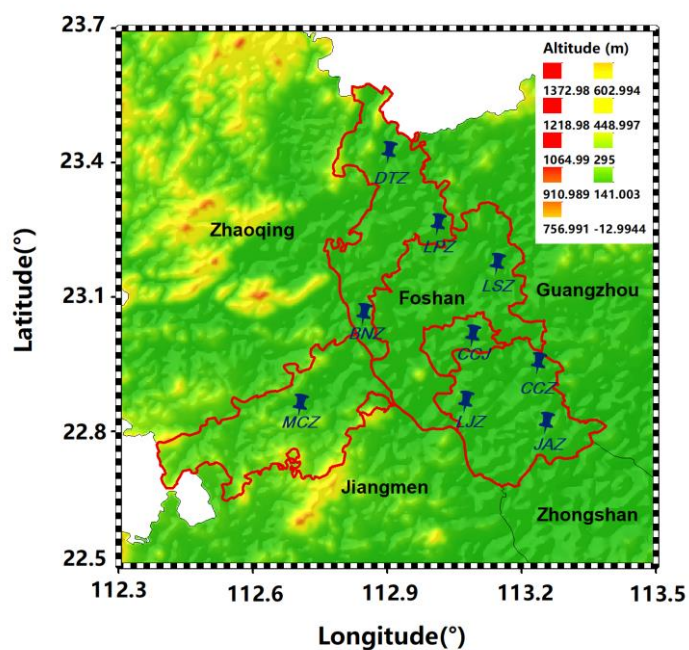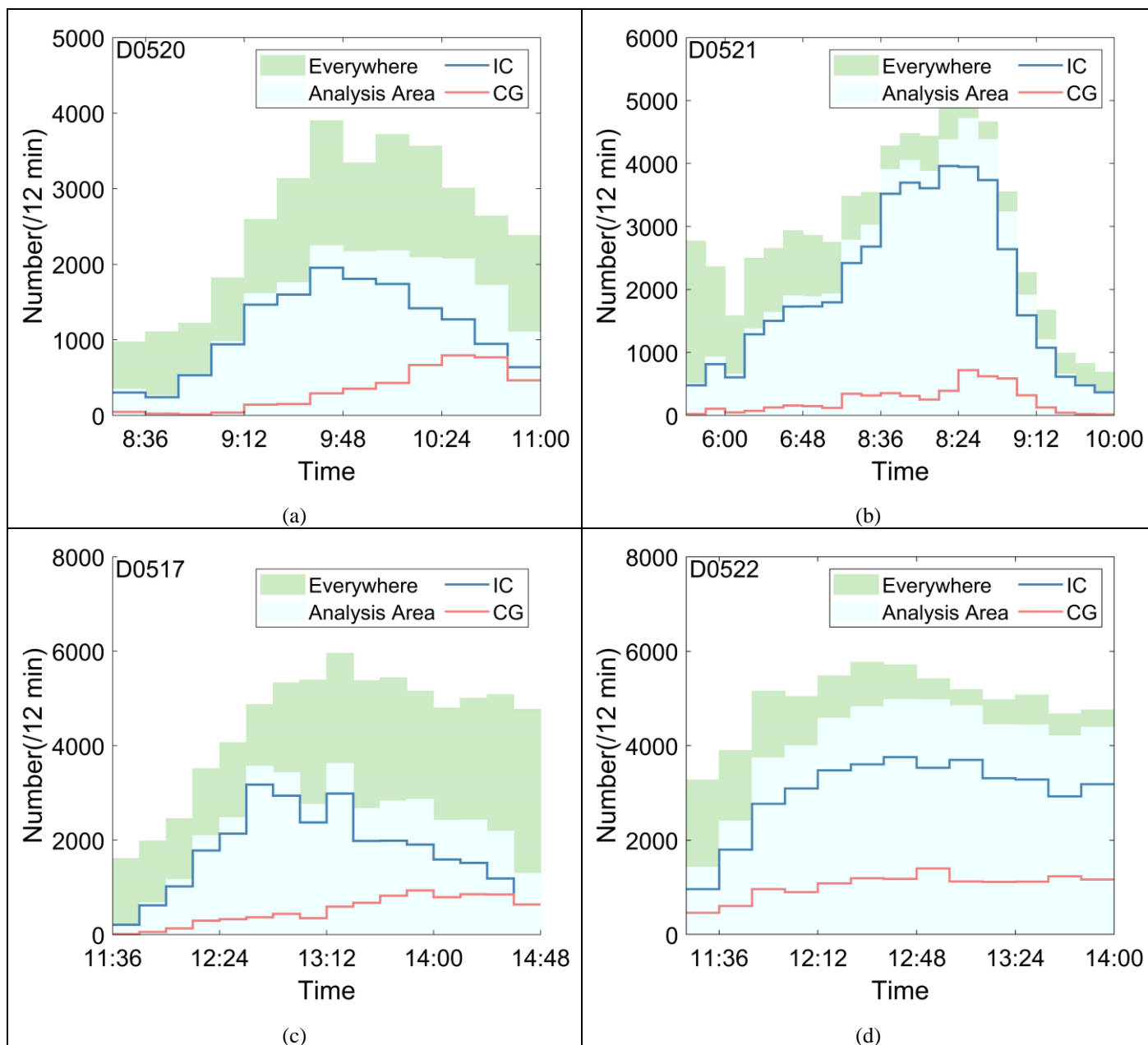
Figure

415 **Figure 1. Geographical distribution of the Foshan Total Lightning Location System (FTLLS), in which a full operation of nine sub-stations in the Foshan area are shown. Sub-station location is displayed by blue icons.**
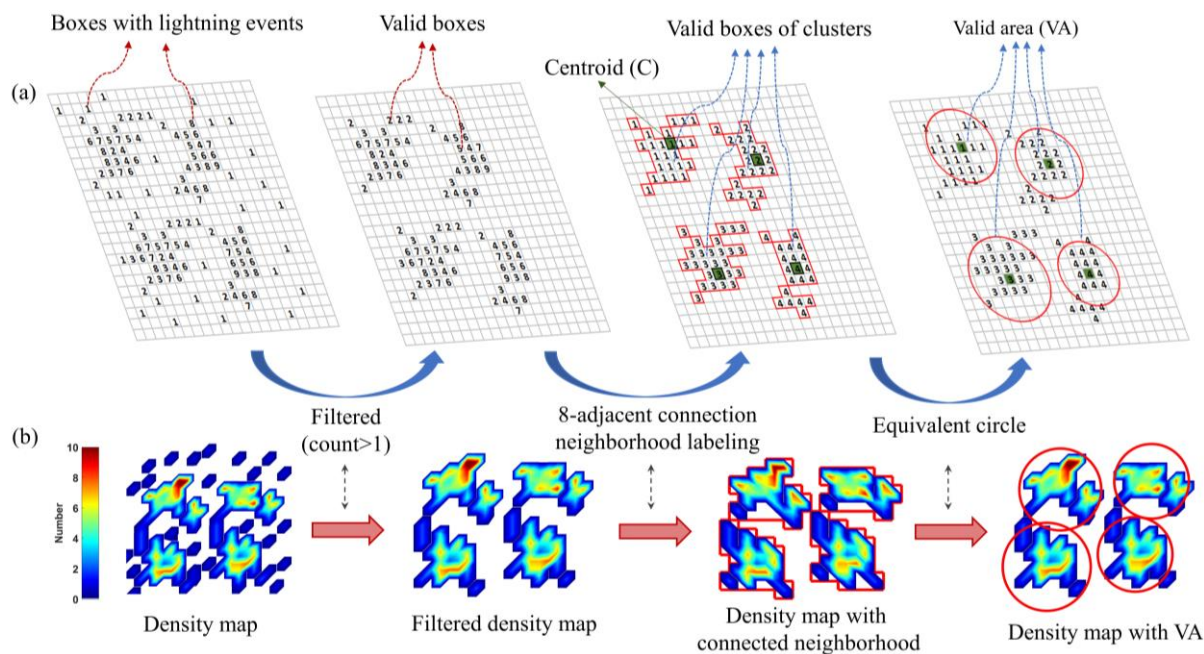
Figure 2. (a) Illustration of the 8-adjacenct connected-neighborhood labeling and the procedure of dealing with the
lightning data to obtain the centroid and the valid area of clusters. (b) The workflow of cluster identification through
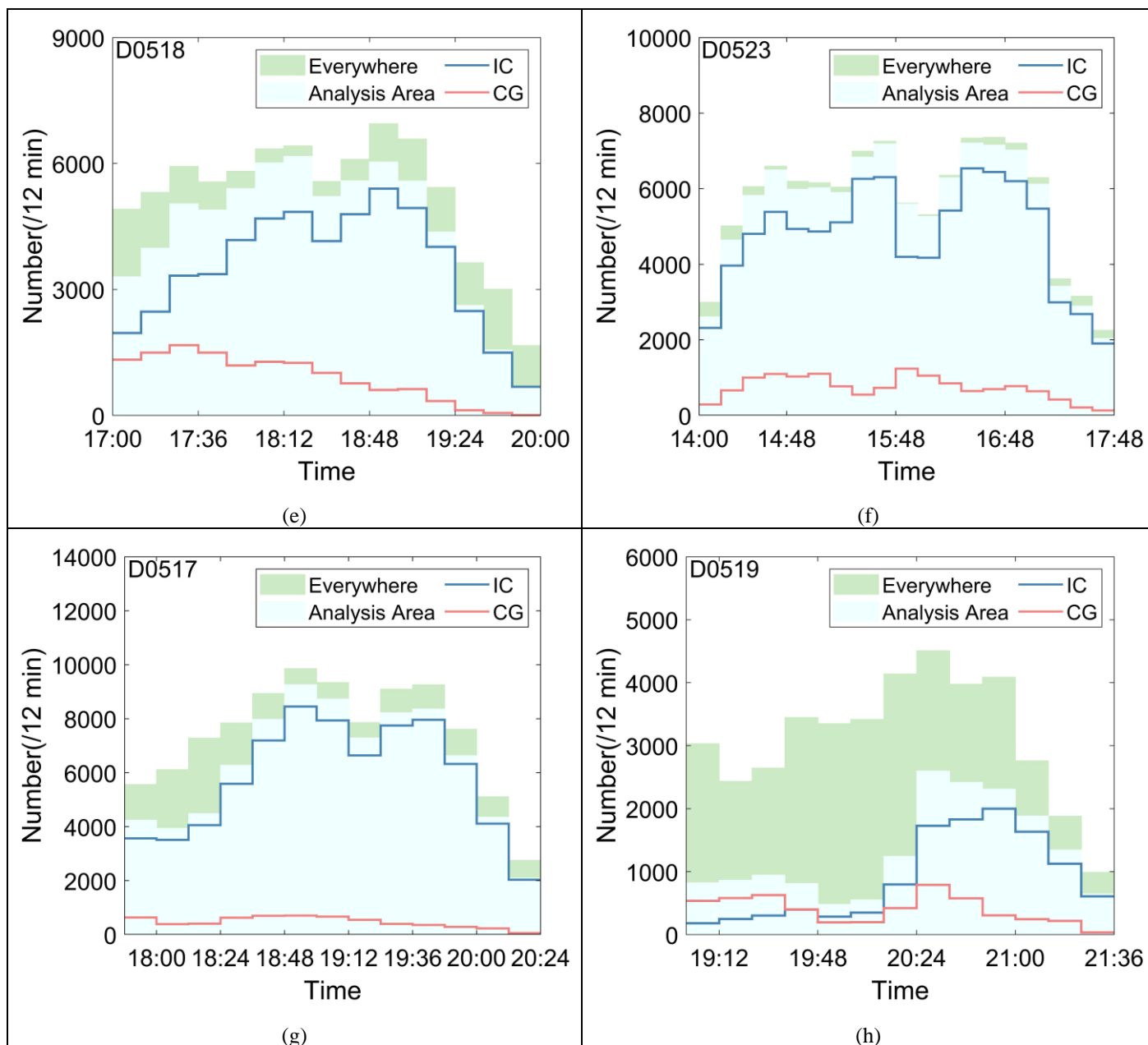**density map.**

425

(a)

(b)

(c)

(d)

Figure 3. (a-h) Life time diagrams of total lightning for thunderstorm case study from 17 May to 23 May. The green shaded areas represent all total lightning events detected by the LLS network, whereas the light blue shaded areas represent total lightning events detected during the thunderstorm processes. The blue and red lines indicate the number of IC events and CG events with respect to time per 12 min, respectively.
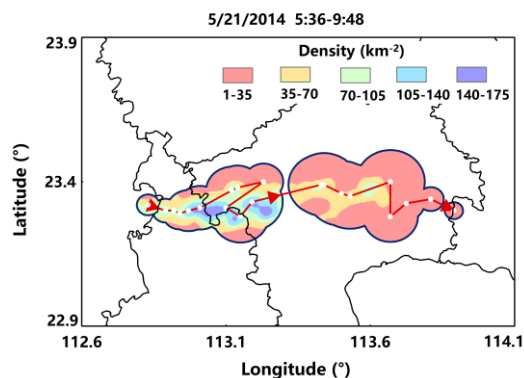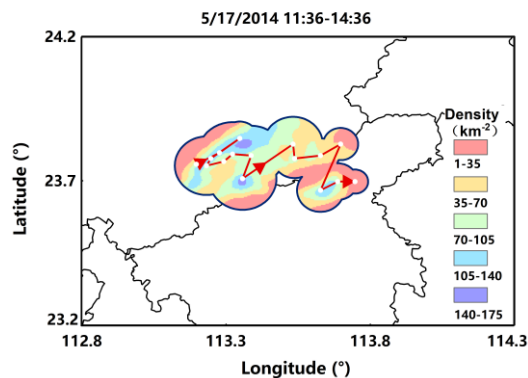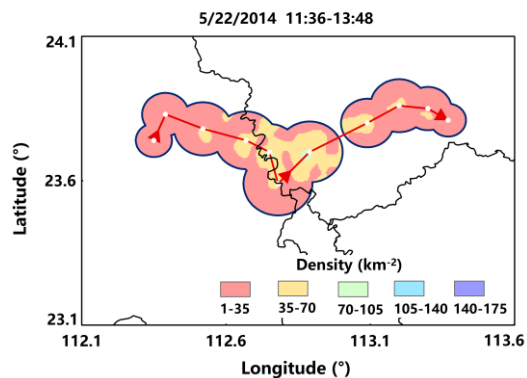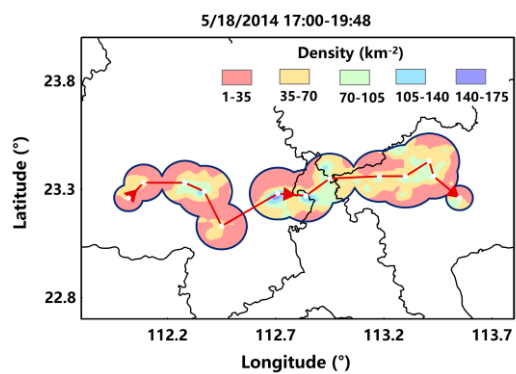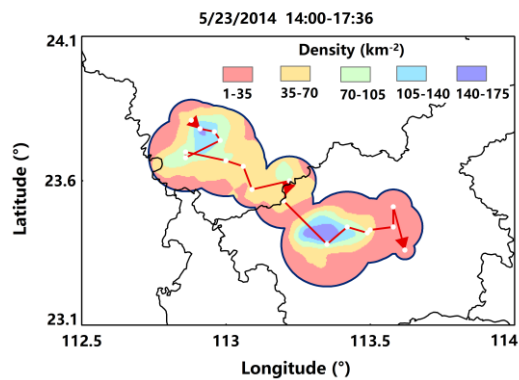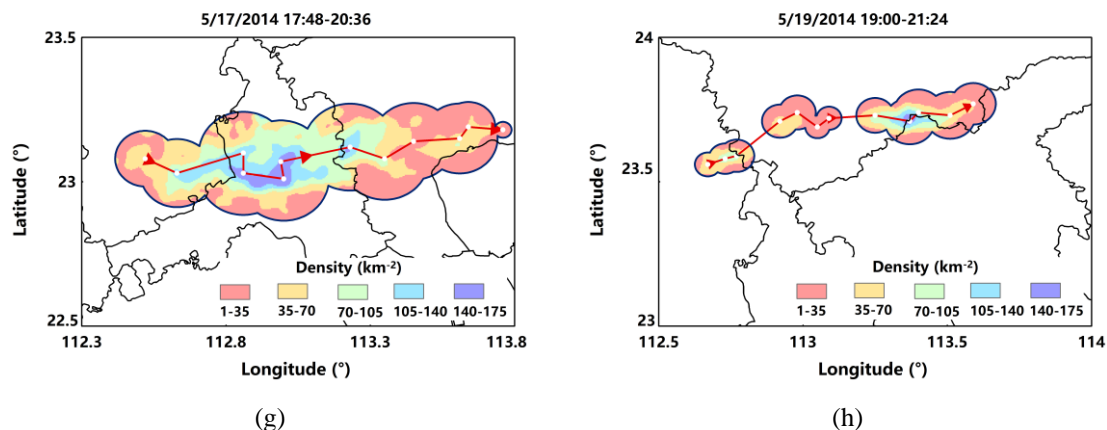
435

(a)

(b)

(c)

(d)

(e)

(f)

(g)

(h)
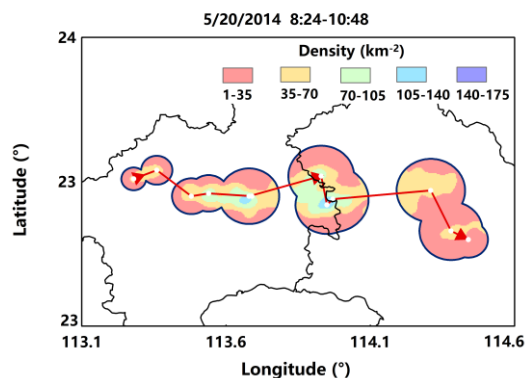
Figure 4. Ground tracks of eight thunderstorms occurred over the Pearl River Delta region in May, 2014. The horizontal axis corresponds to the latitude with the vertical axis standing for the longitude. The white solid dot is the discharge centroid of the valid area in 12 min intervals. Solid red line between two dots is the general path of thunderstorm and the VA that the storms cover is expressed by the centroid-centered circle of a time interval. The lightning density of thunderstorm during the whole process is shown within the valid area.

440

445
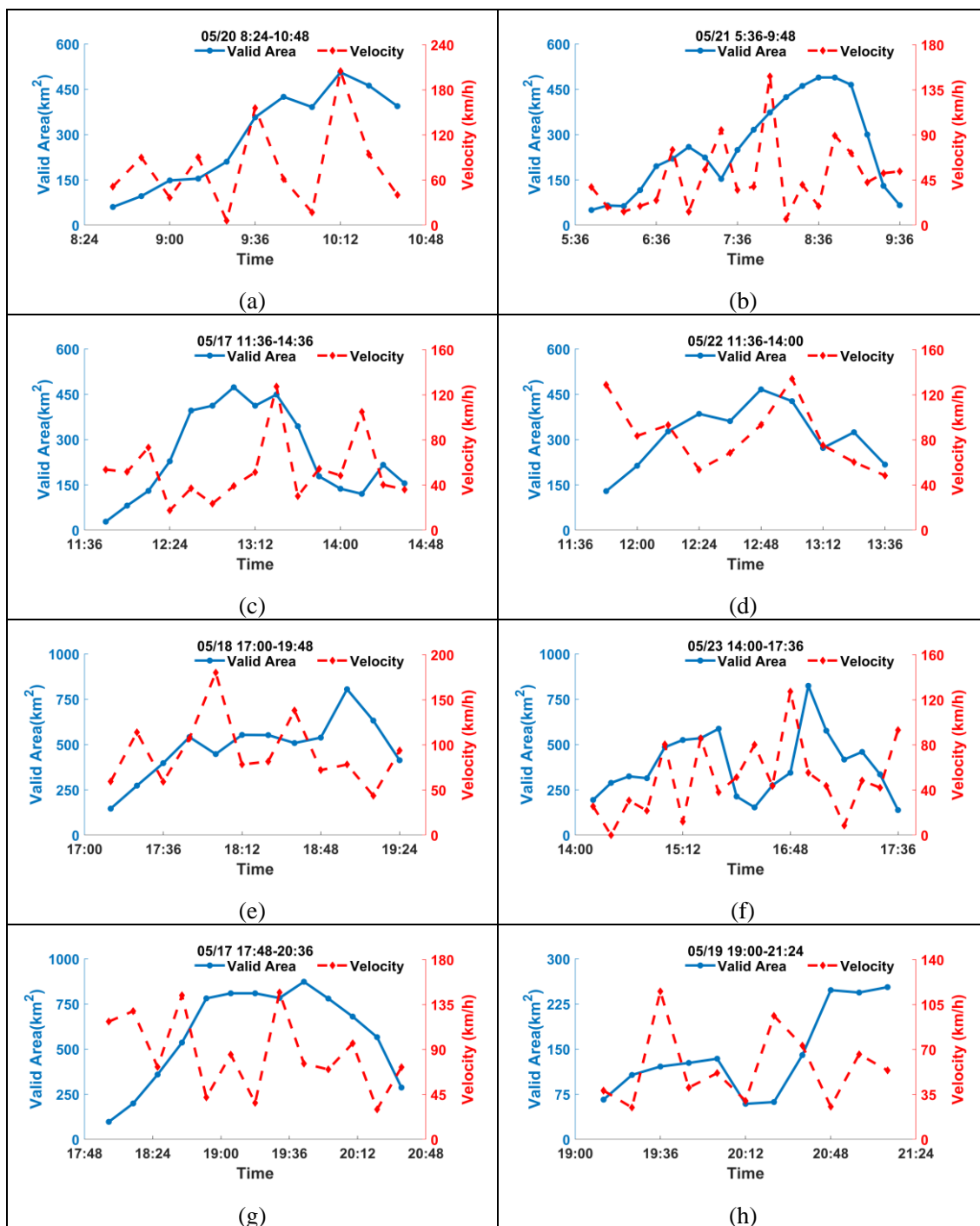
Figure 5. Valid area and velocity of eight cases, as a function of time. The blue solid line and the red dotted line represents the valid area and velocity within a time interval, respectively.
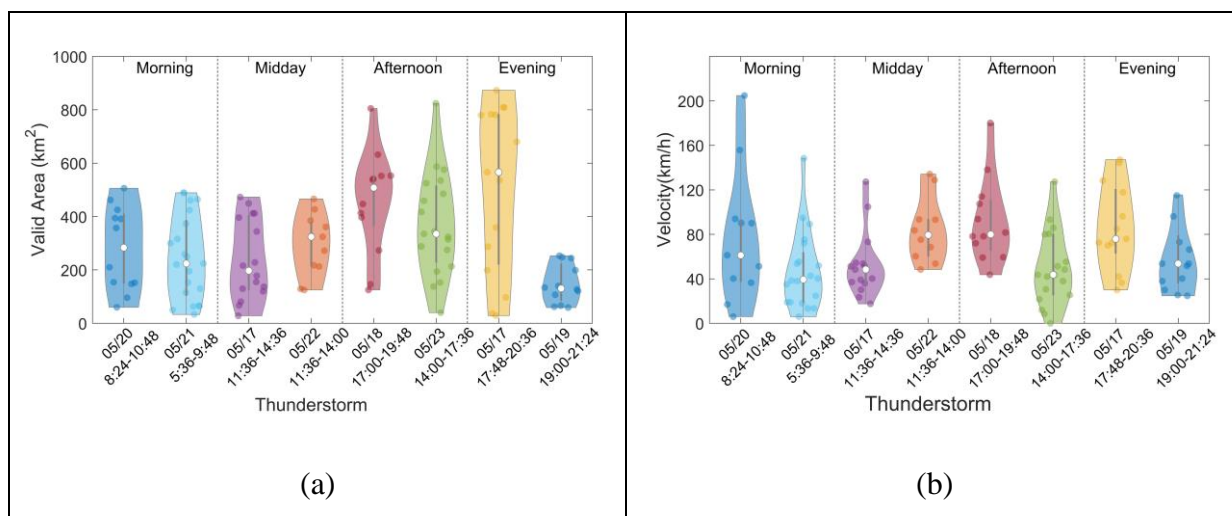
Figure 6. (a) Comparison of valid area between eight cases. The upper and lower edges of boxes mean the maximum and minimum value. The while circle in each box represents the median of VA. The filled circles with darker color than the box represent all VA values of thunderstorms. The grey vertical line in the box represent the interquartile range of VA. (b) Same as (a), but for the velocity.
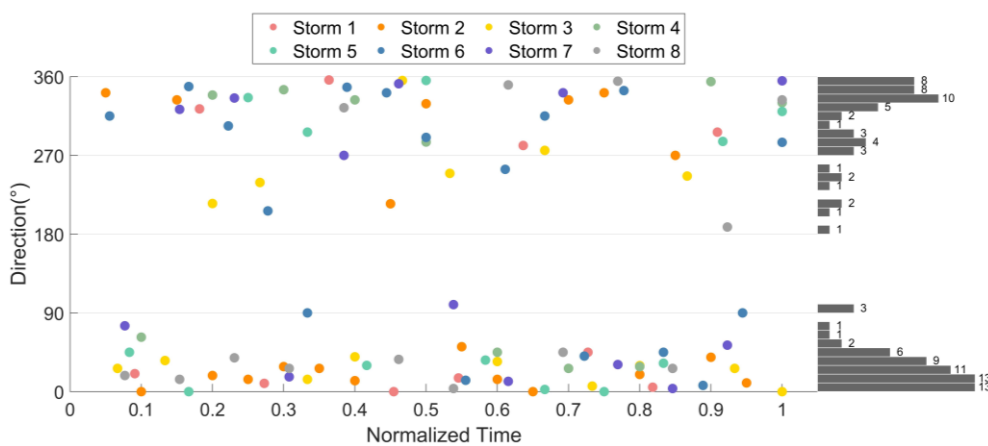
Figure 7. The cluster direction of motion in each interval. The colored dots denote different thunderstorms. As the duration of thunderstorms are different, the normalized time is used for the gathering of all directions of thunderstorm movements. The bar chart on the right represents the frequency of 10° angle range.

21

465

Table 1. Five parameters to characterize the motion of thunderstorms

Parameter	Indication
Duration (h)	The thunderstorm duration of the whole evolution process
Valid area (km^2)	The area that the thunderstorm affects, obtained by the number of valid boxes.
Velocity ($km\ h^{-1}$)	The speed between two centroids.
Direction (°)	The angle of motion, taken the east-west direction as benchmark.
FD_{lon} (km)	The farthest longitudinal distance of centroids during the lifetime of thunderstorm
FD_{lat} (km)	The farthest latitudinal distance of centroids during the lifetime of thunderstorm

470 **Table 2. Overall characteristics of eight thunderstorms occurred within a week**

	Storm	Date	Time (LT)	Total lightning		IC events		CG events		NBEs	
				All	No.$(hour^{-1})^a$	No.	%[b]	No.	%[b]	No.	%[b]
Morning	1	05/20	8:24-10:48	17,985	8,175	14,215	79.0	3,725	20.7	45	0.3
	2	05/21	5:36-9:48	46,681	11,115	41,411	88.7	4,945	10.6	325	0.7
Midday	3	05/17	11:36-14:36	37,418	12,473	28,325	75.7	8,519	22.8	574	1.5
	4	05/22	11:36-14:00	44,694	18,623	33,305	74.5	11,168	25.0	221	0.5
Afternoon	5	05/18	17:00-19:48	65,786	23,495	52,126	79.2	13,250	20.1	410	0.6
	6	05/23	14:00-17:36	101,242	28,123	87,041	86.0	13,558	13.4	643	0.6
Evening	7	05/17	17:48-20:36	81,872	29,240	75,118	91.8	6,028	7.4	726	0.9
	8	05/19	19:00-21:24	17,433	7,263	11,780	78.9	3,007	20.1	139	0.9
Average				51,326	17,278	42,915	81.7	8,025	17.5	385	0.8

Table 3. Parameters to characterize thunderstorms of eight cases.

	Date	Duration (h)	Valid Area (km^2)		Velocity (km h^{-1})		Longitudinal Distance (km)	Latitudinal Distance (km)
			Max	Mean	Max	Mean		
Morning	05/20	2.2	506	279.6	204.8	77.0	116	24
	05/21	4.2	489	244.8	148.4	47.4	106	12
Midday	05/17	3	473	239.1	127.3	52.5	55	18
	05/22	2.4	466	295.1	134.2	83.9	108	27
Afternoon	05/18	2.8	805	456.2	180.1	92.1	153	30
	05/23	3.6	824	369.8	127.3	49.3	76	45
Evening	05/17	2.8	891	662.7	147.1	72.7	146	20
	05/19	2.4	253	146.7	115.3	55.9	92	21
Average		2.93	588.38	336.75	148.06	66.35	106.5	24.63

Table 4 Parameters comparison between the summer thunderstorms in the PRD region and previous studies.

	Data	Threshold	Cases	Duration (h)	Area (km²)	Velocity (km h⁻¹)	Farthest Distance (km)	Direction (°)
This paper	FTLLS	Area > 25 km² Duration >60 min	8 cases	2.93	Mean: 336.75 (in 12 min)	Mean: 66.35	Longitudinal: 106.5 Latitudinal: 24.63	270-360
Betz et al. (2008)	LINET	/	19 June 2007 Cell#8		Max: nealy 1550 (in 10 min)	Max: nealy 90	/	/
			19 June 2007 Cell#3		/	Max: nealy 80		
			21 July 2007 Cell#29		Max: nealy 7000	Max: nealy 60		
			21 July 2007 Cell#51		Max: nealy 2500	Max: nealy 55		
Rigo et al. (2010)	LINET & Radar	>12 dBz Area >24 km² Duration >50 min	66 cases	3.5	Mean: 509 (in 6 min)	/	/	/
Kohn et al. (2011)	ZEUS		Summer (13,600 cases)	/	Max: nealy 3400 (in 15 min)	Mean: 16.5	/	/
			Winter (670 cases)	/	Max: nealy 3700	Mean: 6.2	/	/
Meyer et al. (2013b)	LINET & Radar	Duration >35 min	12 May 2008	/	/	80	Diagonal length: 28	/
			25 June 2008	/	Max: nealy 500 (in 15 min)	/	/	/
Harrison and Karstens (2017)	/	/	9 years in CONUS	/	/	Mean: 45	/	244
Miller and Mote (2017)	Radar	>40 dBz Duration >30 min	Pulse thunderstrom (5378 cases)	2.95	Medium: 470 (in 5 min)	/	/	/
			Weakly forced thunderstorm (885,496 cases)	0.78	Medium: 42 (in 5 min)	/	/	/